Using X-Ray Microtomography for the Three Dimensional Mapping of Minerals

Albina Mutina and Dmitry Koroteev, Schlumberger Moscow Research, Moscow, Russia

BIOGRAPHY

Dr Albina Mutina received her PhD in physics from the Kazan State University, Russia. She is specialized in the nuclear magnetic resonance and X-ray micro tomography for complex fluids and heterogeneous media. With over 40 publications dedicated to the study of oils, porous media and biological objects, she is working now as a Senior Research Scientist at the Schlumberger Moscow Research Center.

ABSTRACT

This study presents an experimental evaluation of the three dimensional (3D) microscale mineral mapping of synthetic multi-mineral powders. We show that X-ray micro-computed tomography (microCT) allows imaging and identification of micrometer-size granules of different minerals in 3D. The possibility of the application of microCT technique for natural samples such as geologic rocks and the limitations of the technique are discussed. The presented results clearly demonstrate that the micro-CT technique together with appropriate algorithms for 3D image processing and information about the total mineral content allow the characterization of mineral distribution inside many types of natural rocks.

KEYWORDS

micro-computed X-ray tomography, 3D mapping, rocks, minerals, image analysis, image processing, anisotropic diffusion filter, edge-preserving smoothing

ACKNOWLEDGEMENTS

The authors thank Alexander Sasov, Alexander Nadeev, Dmitry Korobkov, Sergey Safonov, and Dmitry Miklashevskiy for fruitful scientific discussions.

AUTHOR DETAILS

Dr Dmitry Koroteev,
Schlumberger Moscow Research,
13 Pudovkina Street,
119285 Moscow, Russia,
Tel: +7 495 935 8200 extension 24026
Email: dkoroteev@slb.com

Microscopy and Analysis 26(2):7-12 (AM), 2012

INTRODUCTION

It is well-known that the micro-computed X-ray tomography (micro-CT) technique provides non-destructive reconstruction of virtual slices in which a grayscale represents the X-ray absorption distribution within the object. The absorption (attenuation) depends on the chemical composition of the material, its physical density, and the spectral characteristics of an X-ray source [1]. The range of X-ray energies used in computed tomography (CT) allows X-ray to be transmitted through very dense objects, such as rocks. Therefore X-ray CT techniques give an opportunity for non-destructive examination of internal mineral distribution in the rock samples.

For geological applications, the micro-CT technique is widely used for retrieving the exact pore space microarchitecture [2, 3]. Another well known application is the 3D mapping of metal inclusions in samples of different nature [4, 5]. In both cases, the authors demonstrated perfect capabilities of the imaging technique for distinguishing media with X-ray attenuation coefficients differing by orders of magnitude, such as air-rock or polymer-metal. However, many natural rocks contain minerals with X-ray attenuation coefficients of the same order of magnitude, especially rocks forming oil and gas reservoirs. Precise information about the micro-mineral composition of the rocks will allow the proposing of chemical treatments to influence oil recovery [6]. This work discusses micro-CT capabilities for the non-destructive 3D study of such multi-mineral objects.

It should be noticed that there is a method for non-destructive 3D element mapping of an object based on a combination of micro-CT and X-ray fluorescence techniques, called 3D micro-XRF [7, 8]. There are also a number of methods for surface element mapping, such as Raman scanning microscopy [9], X-ray micro-analysis in scanning electron microscopes [10], etc. All such methods provide only two-dimensional information from the sample's surface and do not allow exploring 3D mineral distributions. They also require serious post-processing and analysis for converting element or molecular maps to a mineral one. Here, we present an imaging-based approach for building 3D mineral maps based on the results of non-destructive micro-CT reconstruction.

MATERIALS AND METHODS

Preparation of Test Powders

Test powders were prepared by mechanical fractionizing of three single-mineral stones: quartz, halite, and calcite. The sizes of the powder grains were mainly in the 50 μm to 600 μm range. The grain size distribution for one of the test powders is presented in Figure 1. This distribution was obtained by the analysis of 3D micro-CT images of the powder. A binarization operation was applied to the image to distinguish grains and the surrounding air. A morphological operation of opening was applied in 3D to separate different grains in space.

The clarity of the chemical composition of the grains was checked by energy-dispersive X-ray (EDX) microanalysis in a scanning electron microscope.

Principle of X-Ray Micro-Computed Tomography

In X-ray micro-CT experiments the object is placed between an X-ray source and an X-ray sensitive detector. The detector acquires projection images of the object's internal microstructure at number of different angular positions by step-like object rotation. Sometimes the object is motionless and multi-angle image acquisition is performed by a step-like rotation of the source-camera system. Follow-

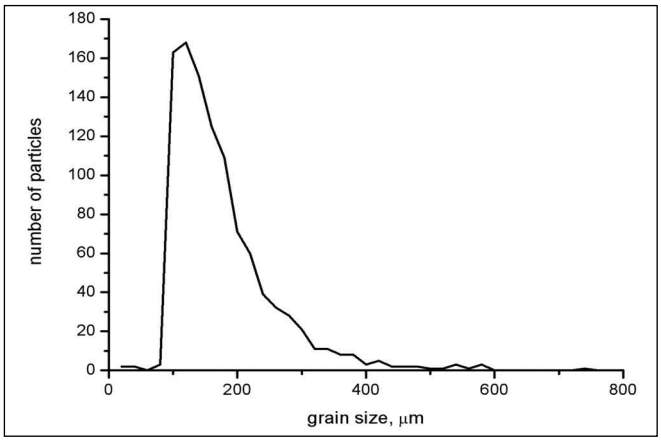

Figure 1:
Grain size distribution of one of the test powders.

ing back projection in computer memory we can reconstruct virtual magnified slices through the object non-destructively.

Experimental: Micro-CT

In our study we used a 1172 micro-CT scanner (SkyScan, Kontich, Belgium). The scanner contained a microfocus X-ray source with a tungsten target, which can operate in the 20-100 keV range of peak energies. By using a thin metal filter, the average energy of the X-ray beam was adjusted to about 30 keV. The instrument included as an X-ray detector a Hamamatsu 11 megapixel cooled CCD camera with a scintillator to convert the X-ray image to visible light. Any object stays on the precision multiaxis manipulator inside the X-ray beam between the source and the detector. The angular projections were acquired using object rotation by this manipulator. In our experiments we acquired 1200 angular projections in every scan.

3D Reconstruction

The 3D image of the object's internal structure was reconstructed using a modified Feldkamp algorithm for cone-beam acquisition geometry [11]. The algorithm is a version of well-known reconstruction technique called filtered back projection (FB) [12]. During such a reconstruction, the raw intensity data are converted to three-dimensional map of attenuation coefficients that have a range determined by the computer system.

Attenuation Coefficients of Minerals

The effective values of the attenuation coefficients for these three minerals were measured before micro-CT scanning of the mixed powder. To measure the effective attenuation coefficients we scanned single grains of each mineral, reconstructed the 3D image and calculated the intensity of X-ray transmission through the grain at particular direction versus length of transmission. The intensity was taken from the projection images, and the transmission length was measured in reconstructed slices.

The typical workflow for measuring the attenuation coefficient for quartz is shown in Figure 2. At the top of Figure 2 there is part of a projection image. The horizontal dashed line shows the position of the reconstructed slice represented below. For each position along the x axis it is possible to acquire intensity $I(x)$ (using the projection image) and transmission length $h(x)$ (using the reconstructed slice). 'Scanning' the projection image and the reconstructed slice from the left to the right allows the calculation of the table function $I(h)$. As is known from the determination of attenuation coefficient (Eq. 1):

$$I(h) = I(0)e^{-\mu h}$$

where μ is the attenuation coefficient.

In other words, the attenuation coefficient might be calculated through the linear regression analysis of $\ln[I(h)/I(0)]$ versus h.

The cone form of an X-ray beam does not influence the result of the regression analysis because it is taken into account during slice reconstruction.

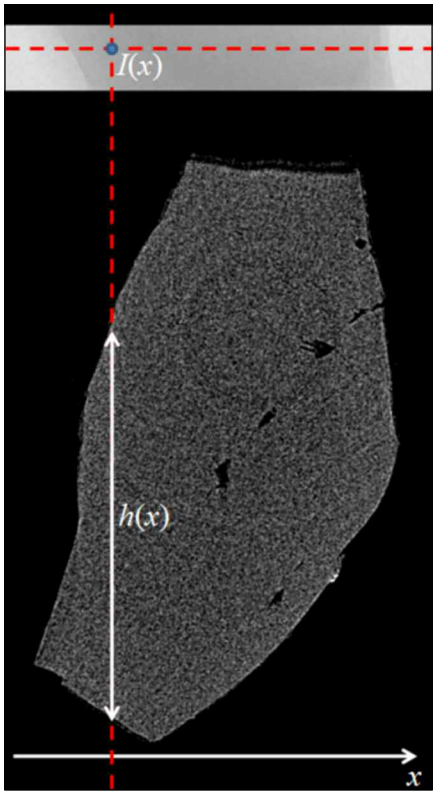

Figure 2:
Example of the workflow for measuring the exact value of an attenuation coefficient of a particular mineral for any particular conditions of the experiment.

Figure 3 (below):
(a) Projection image of test tube with powder.
(b) Vertical cross-section reconstructed by micro-CT.
(c) Direct 3D volume rendering.
(d) Grayscale histogram.

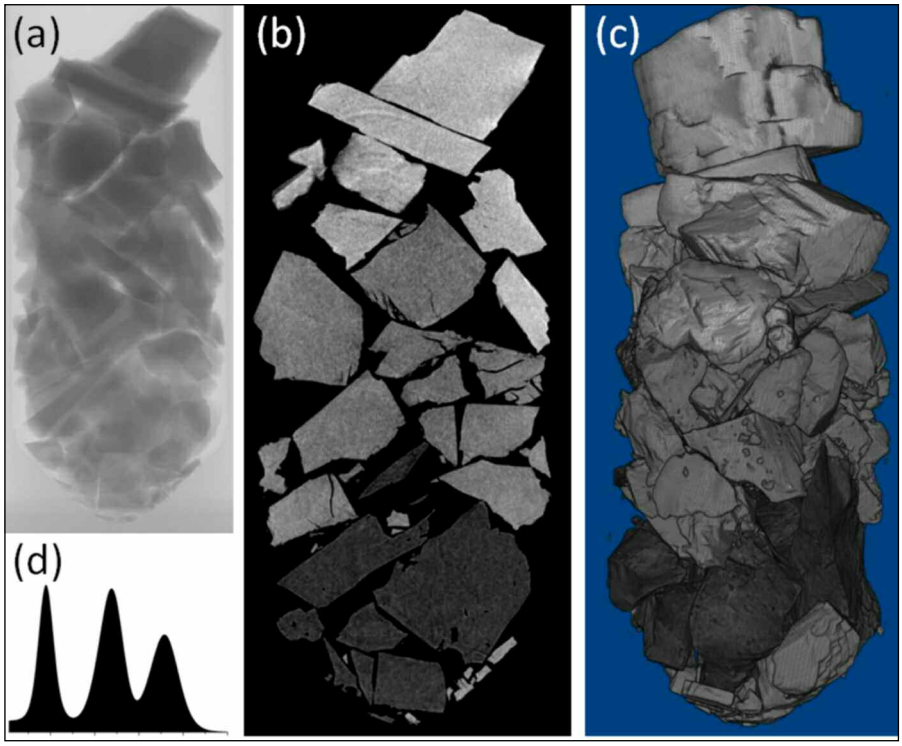

The attenuation coefficients for different minerals can be also found in NIST database [1]. The standard attenuation coefficients in the database calculated for particular energy of monochromatic X-ray radiation and cannot be directly used for experimental set-ups with laboratory polychromatic X-ray sources. We have performed both direct measurements and estimations of the attenuation coefficients using table data from [1]. The results are summarized in Table 1.

The significant differences between the estimated and measured values of the attenuation demonstrates the influence of polychromatic radiation with a complex spectrum. Below we use the measured values of the attenuation coefficients as more adequate data to refer to.

RESULTS AND DISCUSSION

Straightforward Mineral Separation

Micro-tomographical reconstruction of one of the multimineral powder samples is shown in Figure 3. The spatial resolution of the image was 4.6 μm in terms of pixel size. The average grain size for the experiment was 280 μm. The full range of grain sizes was 70-800 μm.

Figure 3a shows one of the projection images of the test tube filled with the powder. Figure 3b demonstrates the reconstructed vertical cross-section of the 3D micro-CT image. Different minerals can be located by differences in grey levels, which correspond to X-ray absorption. The brightest particles are calcite - the mineral with the highest attenuation coefficient. Calcite is mainly located in the top part of Figure 3b. The darkest particles are quartz - the mineral with lowest attenuation coefficient. Quartz is mainly located in the bottom part of Figure 3b. In the central part of the sample there are a few granules of halite which are characterized by medium grayscale range and X-ray attenuation coefficient. Figure 3c shows the 3D volume rendering of the micro-CT results. Figure 3d demonstrates a grayscale histogram from the full reconstructed volume. The histogram has three sharp peaks representing (from left to right): quartz, halite, and calcite. Such separation allows segmenting the 3D image using simple threshoding operations in local minima between peaks. The segmented image (Figure 4 a, b) represents a full 3D mineralogy map of the interior of the sample used in the microtomographic experiment. Figure 4c shows the distribution of the minerals along the vertical axis.

One can note that distances between maxima of histogram peaks in Figure 3d are nearly proportional to the differences of X-ray attenuation values for corresponding minerals. This demonstrates that the micro-CT technique is very linear in reconstruction of X-ray attenuations. One can also note that the minerals with relatively close low values of X-ray attenuation coefficient (namely quartz and halite) are perfectly resolved in the histogram. Different feldspars have X-ray attenuation coefficients in a range which overlaps with the range from quartz to halite. This makes the micro-CT technique very promising for distinguishing quartz and feldspars in natural sandstones.

For the test presented in Figures 4 and 5 we used minerals with attenuation coefficients in the ratio 1:1.3:1.7. The average grain size was about 20 times larger than the effective pixel size of the micro-CT reconstructions and about 100 times larger than the spot size of the X-ray source. Furthermore, we prepared a powder with similar volume fractions for each mineral. These facts led to such a good separation of histogram peaks and allowed simple segmenting of the grayscale image. Without doubt, decreasing average grain size with respect to the pixel size and choosing substances with closer values of X-ray attenuation coefficient, may create complicity in mineral separation. However the sizes of the powder grains in the scanned model sample were of the same order as that of the grains in geological microstructures and far from the resolution limit of the micro-CT technique. This ensured the applicability of the technique for the non-destructive mineral mapping inside real rock samples.

Separation Improvement by Image Processing

The case with more difficult separation of different minerals from the overlapped peaks at grayscale histogram is demonstrated by another micro-CT dataset. A test powder for this experiment contained grains from same three minerals, but the average grain size (160 µm) was nearly twice as small compared that described in the previous case. Overall, the grain size ranged from 20 µm to 700 µm. The spatial resolution for this experiment was 2.5 µm in terms of pixel size.

Figure 5a shows a part of a vertical cross-section of a 3D micro-CT image together with its grayscale histogram. Due to limited signal-to-noise ratio and reconstruction artifacts, peaks in the histogram are obviously not as well separated as in the histogram of the previous case. It is possible to observe certain horizontal gradients of intensity over the grains located at the left side of Figure 5a. This makes an automated segmentation with simple thresholding at local minima not reliable. Performing simple segmentation leads to uncertainty in identification of these three minerals in the

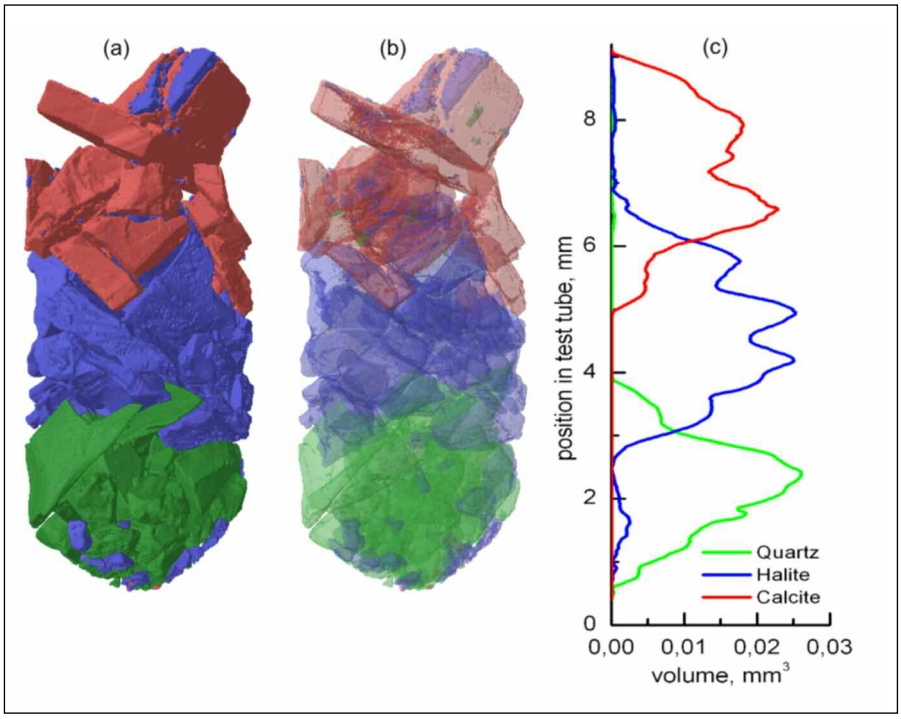

Figure 4:
(a, b) Segmented 3D micro-CT images. (c) The distribution of the minerals along the test tube.

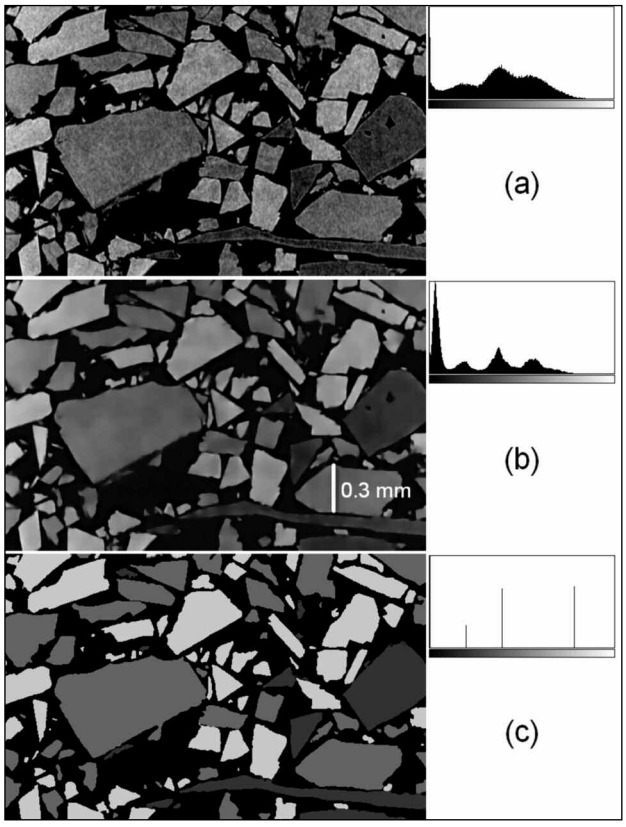

Figure 5:
(a) Part of a vertical cross-section of 3D micro-CT image of multi-mineral powder.
(b) Filtered image.
(c) Segmented image.
On the right there are grayscale histograms of the images.

output image. As a result of segmentation in such a noisy image, every grain will be identified as a mixture of two or even three minerals, which is in contradiction with the sample preparation in this particular case.

To avoid uncertainties from the segmentation process, different pre-processing procedures might be applied. Numerous publications describe using image filters for enhancing peak separation in histograms [13]. Simple smoothing filters (e.g. mean, median or Gaussian) are unusually good at histogram contrast enhancement. But sufficient improvement of peak separation requires a rather big window size, which consequently leads to a significant loss of spatial resolution. That is why to end up with adequate segmentation we have applied a so-called anisotropic diffusion filter, known as a contrast-enhancing edge-preserving tool, for image processing.

In general, diffusion filters represent a physical process that equilibrates disturbed concentration of some substance within a definite volume with time. As is known, diffusion is a mass conservative process. In image processing, grayscale values play the role of concentration, and so the diffusion process can be expressed by the following [14] (Eq. 2):

$$\frac{\partial I(\mathbf{x},t)}{\partial t} = div(G(\mathbf{x},t)\cdot\nabla I(\mathbf{x},t))$$

where $\mathbf{x}$ refers to the image axes (i.e. x, y, z), t refers to the iteration 'time' step, $I(\mathbf{x},t)$ is the grayscale field within the image, and $G(\mathbf{x},t)$ is the diffusivity tensor, designed to steer the direction of the diffusion process. G is a quadratic, positive semidefinite matrix. The diffusion equation 2 can be solved numerically using finite differences. Usually the term

$$\frac{\partial I(\mathbf{x},t)}{\partial t}$$

is replaced by an Euler forward difference approximation [15] (Eq. 3):

$$I(\mathbf{x},t+\tau) = I(\mathbf{x},t) + \tau\cdot I(\mathbf{x},t)\frac{\partial I(\mathbf{x},t)}{\partial t}$$

where τ denotes the 'time step' size.

To preserve the edges the diffusion smoothing is made depending on strength and direction of the grayscale gradient. The diffusion tensor G is therefore defined as a function of the structure tensor (Eq. 4):

$$G = \begin{bmatrix} v_1 & v_2 & v_3 \end{bmatrix} \times \begin{bmatrix} \lambda_1 & 0 & 0 \\ 0 & \lambda_2 & 0 \\ 0 & 0 & \lambda_3 \end{bmatrix} \times \begin{bmatrix} v_1 \\ v_2 \\ v_3 \end{bmatrix}$$

where v_i denotes the eigenvectors of the structure tensor. The eigenvalues λ_i define the strength of the smoothing along the direction of the corresponding eigenvector v_i. The values of λ_i rank from 0, which stands for no smoothing, to 1, which stands for strong smoothing.

Therefore, this approach allows performing anisotropic smoothing with respect to the eigenvectors determined from the local structure of the image. That's why the method of anisotropic diffusion is treated as one of the most useful for preserving internal architecture of an image.

	Quartz	Halite	Calcite
Chemical Formula	SiO_2	NaCl	$CaCO_3$
Density, g cm^{-3}	2.6	2.2	2.7
Attenuation Coefficient, cm^{-1} Estimated from data in [1]	2.3	3.9	5.0
Measured Attenuation Coefficient, cm^{-1}	1.486±0.005	1.988±0.009	2.592±0.014

Table 1:
The chemical and physical characteristics of the minerals involved in the CT experiments.

Figure 5b illustrates an example of application of the anisotropic diffusion filter to the micro-CT dataset shown in Figure 5a. The right panel of Figure 5b shows a histogram of the filtered image with improved peak separation, which already allows automated thresholding at local minima to get appropriate four phase segmentation of filtered image. Peaks at the histogram stand for (from left to right): air, quartz, halite and calcite. Comparison of the histograms in Figure 5a and Figure 5b clearly shows that applying anisotropic diffusion filter have not affected the position of the peaks. As in the previous case, the distances between maxima of 'mineral' histogram peaks are nearly proportional to the differences of X-ray attenuation values for corresponding minerals at both original and filtered images.

The thresholding at local minima together with despeckling operations and morphological operation of opening allows the creation of a segmented image presented in Figure 5c. The histogram in the right panel of Figure 5c represents four vertical lines corresponding to air and the three described minerals. Note that the gray scales of the segmented image were chosen for better visualization of differences between the phases (minerals) and have no link with the attenuation coefficients of the minerals presenting in the test powder.

CONCLUSIONS

We have conducted test experiments to study the feasibility of using an X-ray micr-computed tomography technique to distinguish different minerals inside 3D objects, such as rock, using a non-destructive micro-CT technique. Our results demonstrate that existing commercial micro-CT instruments can be used for distinguishing minerals with relatively small difference in X-ray attenuation coefficients. Minerals with close and relatively low values of X-ray attenuation coefficients were perfectly resolved in the model of mixed mineral powder.

A case when the reconstructed micro-CT image presents a clear multi-peak grayscale histogram allows simple segmenting of the different minerals, i.e. the building of a 3D mineral map directly from a micro-CT reconstruction. When the resulting micro-CT 3D images contain significant noise and/or artifacts, an appropriate image pre-processing can be applied to perform adequate image segmentation for mapping.

REFERENCES

1. *Saloman, E. B., Hubbell, J. H., Scofield, J. H. Atomic Data and Nuclear Data Tables 38, 1988.*
2. *Silin, D., Tomutsa, L., Benson, S. M., Patzek, T. W. Microtomography and pore-scale modeling of two-phase fluid distribution. Transport in Porous Media, published online August 11, 2010.*
3. *Siddiqui, S., Sarker, M. R. H. Trends in CT-scanning of reservoir rocks. Proc. Advances in Computed Tomography for Geomaterials, 206-212, 2010.*
4. *Clyne, T. W., Markaki, A. E., Tan, J. C. Mechanical and magnetic properties of metal fibre networks, with and without a polymeric matrix, Composites Science and Technology 65:2492-2499, 2005.*
5. *Masschaelea, B., Baechlerb, S. , Cauwelsa, P., Cloetensc, P., Diericka, M., Jolieb, J. , Mondelaersa, W. Element sensitive X-ray micro tomography for determination of the metal diffusion in teeth with amalgam fillings. Radiation Physics and Chemistry 61:625-626, 2001.*
6. *Morrow, N. R. Wettability and its effect on oil recovery, Journal of Petroleum Technology 42:1476-1484, 1990.*
7. *Boone, M. N., Dewanckele, J. , Cnudde, V., Silversmit, G., Van Hoorebeke, L., Vincze, L., Jacobs, P. Combination of laboratory micro-CT and micro-XRF on geological objects. Proc. Advances in Computed Tomography for Geomaterials 189-196, 2010.*
8. *Sasov, A., Liu, X., Rushmer, D. Compact micro-CTImicro-XRF system for non-destructive 3D analysis of internal chemical composition. Proc. 14th European Microscopy Congress I4 705-706, 2008.*
9. *Haskin, L. A., Wang, A., Rockow, K. M., Jolliff, B. L. Raman spectroscopy for mineral identification and quantification for in situ planetary surface analysis: A point count method. Journal of Geophysical Research 102:19293, 2007.*
10. *Ying, G. Automated Scanning Electron Microscope Based Mineral Liberation Analysis, Journal of Minerals & Materials Characterization & Engineering 2:33-41, 2003.*
11. *Feldkamp, L.A., Davis, L. C., Kress, J. W. Practical conebeam algorithm. Journal of the Optical Society of America 1:612-619, 1984.*
12. *Herman, G. T. Fundamentals of computerized tomography: Image reconstruction from projection. 2nd Ed, Springer 2009.*
13. *Mitra, S. K., Sicuranza, G. L. Nonlinear image processing. Academic Press 2001.*
14. *Frangakis, A. S., Stoschek, A., Hegerl, R. Wavelet transform filtering and nonlinear anisotropic diffusion assessed for signal reconstruction performance on multidimensional biomedical data. IEEE Transactions on Biomedical Engineering 48:213-222, 2001.*
15. *Tabik, S., Garzon, E.M., Garcia, I., Fernandez, J. J. Implementation of Anisotropic Nonlinear Diffusion for Filtering 3D Images in Structural Biology on SMP Clusters. John von Neumann Institute for Computing, NIC Series 33:727-734, 2006.*